Journal of Sound and Vibration 325 (2009) 950–958

Contents lists available at ScienceDirect

Journal of Sound and Vibration

journal homepage: www.elsevier.com/locate/jsvi

Transient growth rates of near-grazing impact velocities: Theory and experiments

Bryan Wilcox [a,*], Fredrik Svahn [b], Harry Dankowicz [a], Jenny Jerrelind [b]

[a] Department of Mechanical Science and Engineering, MC 244, University of Illinois at Urbana-Champaign, Urbana, IL 61801, USA
[b] Department of Aeronautical and Vehicle Engineering, Royal Institute of Technology, SE-100 44 Stockholm, Sweden

ARTICLE INFO

Article history:
Received 15 September 2008
Received in revised form
15 January 2009
Accepted 8 April 2009
Handling Editor: C.L. Morfey
Available online 19 May 2009

ABSTRACT

In this paper, nonsmooth fold bifurcations associated with the onset of low-relative-velocity (near-grazing) impacts in an oscillatory mechanical system are proposed as a potential operating principle for high-speed limit switches. Specifically, analytical, numerical, and experimental methods are employed to investigate the near-grazing transient behavior in a representative system. It is shown that the rate of growth of successive impact velocities increases beyond all bounds as the threshold parameter value is approached. A limit switch based on the proposed nonsmooth fold scenario would thus be expected to outperform one that relies on a smooth bifurcation, such as the cyclic-fold bifurcation, in terms of switching speed and sensitivity.

1. Introduction

Limit switches constitute a class of input–output devices that change operating state in reaction to the crossing of a threshold value of their input [1]. They can be used as indicators, control devices, or more commonly both. Resettable limit switches often include hysteresis to prevent hunting near the threshold. Their use enables the safe, reliable operation of many everyday household items, such as coffee makers, electric circuit breakers, and water heaters. As indicators, limit switches provide a logic high when a set level of a quantity has been reached. These are used to monitor critical values of temperature, voltage, pressure, etc. in both consumer and industrial settings [2–5]. As control devices, limit switches provide the simplest form of feedback: discrete on/off states in response to input. The switch might be permanent, such as when a fuse burns out, or capable of being reset, such as with a circuit breaker.

Of particular interest in the present context are limit switches whose function relies on a snap-like action [6,7]. Within a dynamical-systems context, the internal state of the switch transitions abruptly between two dissimilar steady-state behaviors as a result of a small change in the value of a system parameter. Specifically, as the parameter exceeds the critical value, there is an associated loss of stability or disappearance of the original steady-state behavior. This leaves the limit switch no choice but to evolve to a different steady-state attractor. Examples of such bifurcations, such as saddle-node and subcritical pitchfork bifurcations of equilibria, are exploited in existing limit-switch devices. In these cases, parameter hysteresis typically results from the persistence of the target steady-state behavior even as the system parameter is reduced past the original threshold value. The speed of the transients following the bifurcation and the nature of the input dynamics determine the switch's reaction to excursions past the threshold. As an example, a slow-blow fuse is designed to pass overload currents for a short amount of time to allow for start-up transients in electrical machinery. A lag in switching

* Corresponding author.
E-mail addresses: bwilcox2@illinois.edu (B. Wilcox), danko@illinois.edu (H. Dankowicz).

0022-460X/$ - see front matter © 2009 Elsevier Ltd. All rights reserved.
doi:10.1016/j.jsv.2009.04.012

speed is thus critical to the slow-blow fuse's successful operation. In contrast, in the case of protection for a circuit board containing delicate components, a similar lag in switching speed would be disastrous.

Generalizations to periodic steady-state attractors of the snap-like action due to saddle-node bifurcations of equilibria have been proposed recently for limit-switch design using nonlinear circuitry as well as parametrically excited microelectromechanical devices [8–16]. The corresponding cyclic-fold bifurcation is characterized by the mutual annihilation of a stable and unstable periodic trajectory beyond the threshold value. Using center-manifold theory and the theory of normal forms, the local dynamics in the vicinity of a cyclic-fold bifurcation may be described by the discrete map

$$x_{n+1} = x_n + \mu + x_n^2, \tag{1}$$

where μ denotes the deviation of the system parameter from the threshold value and x_n and x_{n+1} parametrize the deviation from the periodic trajectory at $\mu = 0$ upon successive intersections of a state-space trajectory with a suitably defined Poincaré surface [17]. Here, $x_{n+1} = x_n = x_*$ for some μ corresponds to a periodic response of the continuous state of the device. In particular, it follows that there exist two such periodic responses with $x_* \approx 0$ for $\mu \lesssim 0$, one when $\mu = 0$, and none for $\mu \gtrsim 0$. Specifically, for $0 < \mu, |x_0| \ll 1$ deviations away from the original periodic trajectory grow linearly with n, for sufficiently small n.

The purpose of this paper is to investigate the nonsmooth fold associated with a grazing bifurcation in a vibro-impacting mechanical system for use in limit-switch design [18,19]. As demonstrated below, this alternative compares favorably with the cyclic-fold bifurcation in terms of the growth rate of deviations away from the original periodic trajectory, indicating the potential to ensure a quicker switch response. Here, at the critical threshold value, there exists a periodic oscillation of an internal element of the device that achieves zero-relative-velocity (grazing) contact with a rigid obstacle at some phase of the oscillation. Computable conditions distinguish between the case in which a steady-state attractor persists in the neighborhood of the grazing periodic oscillation for nearby parameter values and the case of interest here, in which the disappearance of a local attractor results in a rapid transition to a distinctly different steady-state behavior. Indeed, as shown using the theory of discontinuity mappings [20,21] and rederived here in terms of successive values of the relative velocity at impact, the growth rate of deviations away from the grazing oscillation increases beyond all bounds as the threshold parameter value is approached.

The paper is organized as follows. Section 2 describes an experimental setup used to explore the near-grazing dynamics and, specifically, the growth of relative velocity at successive impacts. An approximate map describing the relationship between successive values of the relative impact velocity is rigorously derived and validated against numerical simulations in Section 3. Section 4 reports on collected experimental data and compares the observed behavior to the theoretical predictions. Finally, the paper concludes with a discussion summarizing key findings and implications for further work.

2. Phenomenology

2.1. Experimental apparatus

An experimental impacting mechanical system, shown schematically in Fig. 1, was chosen to investigate the transient dynamics following the onset of low-velocity impacts (cf. Refs. [22–27]). The system consists of a spherical steel ball attached to the end of a cantilevered beam. The ball and beam assembly is in turn clamped to a support and oriented as shown in Fig. 1 with the ball resting in front of the head of a Brüel and Kjær Type 4809 electromagnetic shaker. When the shaker is excited (a signal generator and a Brüel and Kjær Type 2706 power amplifier were used), the head moves relative to the body, which is stationary relative to the support. With sufficient excitation amplitude, the head of the shaker will impact the ball resulting in the behavior of interest.

A Polytec PDV100 laser vibrometer was used to gather velocity data. The laser was mounted on a tripod and aimed axially with the motion of the ball. The laser beam was passed through small holes in the support so as to reflect off the objects of interest on the other side (the head and ball), as shown in Fig. 1. Signal generation, data acquisition, and signal processing were performed using a Spectral Dynamics SigLab Model 20–42 Dynamic Signal Analyzer and SigLab software (running in Matlab). For further discussion regarding the experimental apparatus, see Ref. [28].

2.2. Experimental procedure and data processing

To investigate the transient behavior experimentally, a sinusoidal signal was generated using the Virtual Function Generator (VFG) supplied with SigLab. The output from the VFG was routed into an amplifier, then from the amplifier to the inputs of the shaker, again shown schematically in Fig. 1. The shaker was started from rest and the gain of the amplifier increased manually until the amplitude of the shaker oscillations brought the head of the shaker close to the ball.

To get as close as possible to grazing contact, the input signal was then incremented quasi-statically using the digital controls within SigLab until impacting behavior was observed. The amplitude of the increments was the minimal amount possible within SigLab, corresponding to approximately 0.26% of the full-scale input. Subsequent to the onset of impacts,

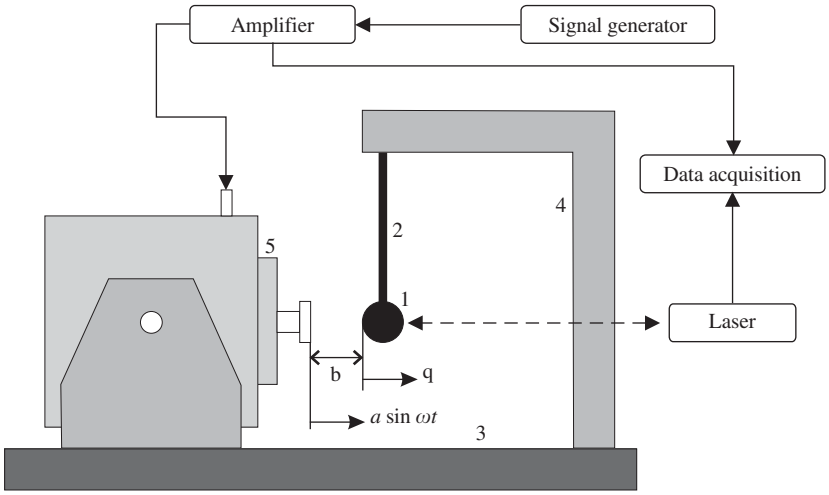

Fig. 1. Schematic of the experimental apparatus used for investigating near-grazing transient dynamics. The system consists of a spherical steel ball (1) attached to the end of a cantilevered beam (2), clamped to a base (3) through a rigid support (4), and oriented such that the ball rests in front of the head of an electromagnetic shaker (5).

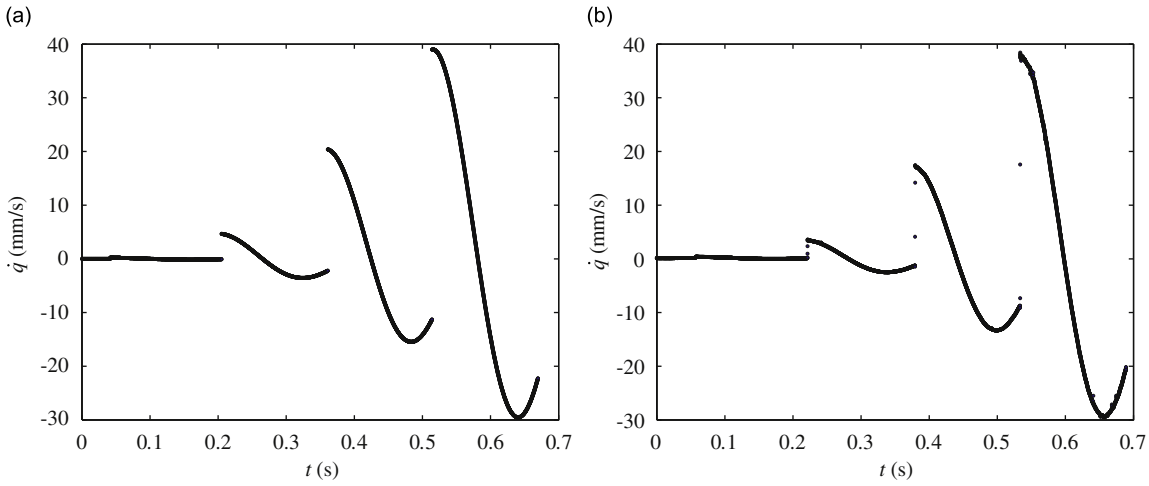

Fig. 2. Characteristic time evolutions for the ball velocity subsequent to the onset of impacts: (a) numerical simulation and (b) experiment.

data were sampled at 12.8 kHz for approximately 30 cycles of the excitation. A characteristic time evolution is shown in Fig. 2(b) and demonstrates the anticipated dramatic growth of the ball velocity over time.

2.3. Mathematical model

Consider, for simplicity, a lumped parameter model of the experimental apparatus in which the ball and beam assembly is represented by a massive particle constrained to straight-line motion and affected by a linear restoring force and damping. Specifically, let q be the displacement of the particle away from its equilibrium position and suppose that $-b+a\sin\omega t$, where $a,b,\omega>0$, represents the displacement of the shaker head relative to the particle's equilibrium position.

Let

$$\mathbf{x}=(q\ \ \dot{q}\ \ \theta=\omega t \bmod 2\pi)^{\mathrm{T}} \tag{2}$$

denote the state of the corresponding hybrid dynamical system with continuous dynamics governed by the smooth vector field

$$\mathbf{f}(\mathbf{x})=(\dot{q}\ \ -2\zeta\omega_n\dot{q}-\omega_n^2 q\ \ \omega)^{\mathrm{T}} \tag{3}$$

as long as

$$h_{\text{impact}}(\mathbf{x}) \stackrel{\text{def}}{=} q + b - a\sin\theta \geqslant 0, \tag{4}$$

and discrete jumps given by

$$\mathbf{x} \mapsto \mathbf{g}(\mathbf{x}) = (q \quad -e\dot{q} + (1+e)a\omega\cos\theta \quad \theta)^{\mathrm{T}} \tag{5}$$

triggered by transversal crossings of the zero-level surface of h_{impact}. Here, ζ is the damping factor, ω_n is the natural frequency of the system, and e represents a coefficient of restitution. In particular,

$$h_{\text{turning}}(\mathbf{x}) \stackrel{\text{def}}{=} \partial_{\mathbf{x}} h_{\text{impact}}(\mathbf{x}) \cdot \mathbf{f}(\mathbf{x}) = \dot{q} - a\omega\cos\theta \tag{6}$$

denotes the rate of change of h_{impact} along trajectories of the smooth vector field, i.e., the relative velocity between the particle and shaker. From the expression for $\mathbf{g}$ it follows that

$$h_{\text{turning}}(\mathbf{g}(\mathbf{x})) = -e h_{\text{turning}}(\mathbf{x}) \tag{7}$$

and thus that trajectories that reach $h_{\text{impact}} = 0$ at *incoming points* with $h_{\text{turning}} < 0$ are connected to trajectories based at *outgoing points* on $h_{\text{impact}} = 0$ with $h_{\text{turning}} > 0$.

2.4. Numerical simulations

A free vibration test of the ball and beam assembly was completed to characterize the damping factor ζ and natural frequency ω_n. The ball was given an initial displacement and released from rest. The transient dynamics of the system were then captured as the system settled to equilibrium. From experimental data averaged over 10 runs and using the method of logarithmic decrement, ζ was estimated at 0.0881 and ω_n was estimated at 25.2 rad/s.

As the collected data were limited to the absolute velocity of the ball, it was necessary to rely on indirect methods for determining a suitable numerical estimate of the coefficient of restitution e. Specifically, e was estimated at 0.55 so as to result in close agreement between the resultant simulated velocity data (shown in Fig. 2(a)) and the experimental data (shown in Fig. 2(b)).

3. Theoretical analysis

3.1. Near-grazing dynamics

As long as $a \leqslant b$,

$$\mathbf{x}(t) = (0 \quad 0 \quad \omega t \bmod 2\pi)^{\mathrm{T}} \tag{8}$$

describes a smooth periodic trajectory of the hybrid dynamical system. In particular, for $a = a^* \stackrel{\text{def}}{=} b$ a simple tangential (*grazing*) contact occurs between this trajectory and $h_{\text{impact}} = 0$ at

$$\mathbf{x}^* = \left(0 \quad 0 \quad \frac{\pi}{2}\right)^{\mathrm{T}}. \tag{9}$$

Here, $h_{\text{turning}}(\mathbf{x}^*) = 0$. Of interest in the subsequent analysis is the dynamics of nearby initial conditions for $a \approx a^*$.

Specifically, let $a - a^* = \varepsilon\delta a$ and consider the initial condition

$$\mathbf{x}_0 = \mathbf{x}^* + \varepsilon\left(\delta a \quad \delta\dot{q} \quad \frac{\delta h_{\text{turning}} - \delta\dot{q}}{b\omega}\right)^{\mathrm{T}} + \mathcal{O}(\varepsilon^2) \tag{10}$$

such that $h_{\text{impact}}(\mathbf{x}_0) = \mathcal{O}(\varepsilon^2)$ and $h_{\text{turning}}(\mathbf{x}_0) = \varepsilon\delta h_{\text{turning}} + \mathcal{O}(\varepsilon^2)$, where $\delta h_{\text{turning}} < 0$ (cf. Fig. 3). It follows that

$$\mathbf{x}_1 = \mathbf{g}(\mathbf{x}_0) = \mathbf{x}^* + \varepsilon\left(\delta a \quad \delta\dot{q} - (1+e)\delta h_{\text{turning}} \quad \frac{\delta h_{\text{turning}} - \delta\dot{q}}{b\omega}\right)^{\mathrm{T}} + \mathcal{O}(\varepsilon^2) \tag{11}$$

such that $h_{\text{impact}}(\mathbf{x}_1) = \mathcal{O}(\varepsilon^2)$ and $h_{\text{turning}}(\mathbf{x}_1) = -\varepsilon e\delta h_{\text{turning}} + \mathcal{O}(\varepsilon^2)$.

In the case that $\zeta < 1$, the smooth flow corresponding to the vector field $\mathbf{f}$ is given by

$$\boldsymbol{\phi}(t, \tilde{\mathbf{x}}) = \begin{pmatrix} \dfrac{\mathrm{e}^{-t\zeta\omega_n}}{\Omega}(\tilde{q}\Omega\cos\Omega t + (\dot{\tilde{q}} + \tilde{q}\zeta\omega_n)\sin\Omega t) \\ \dfrac{\mathrm{e}^{-t\zeta\omega_n}}{\Omega}(\dot{\tilde{q}}\Omega\cos\Omega t - \omega_n(\dot{\tilde{q}}\zeta + \tilde{q}\omega_n)\sin\Omega t) \\ \tilde{\theta} + \omega t \end{pmatrix}, \tag{12}$$

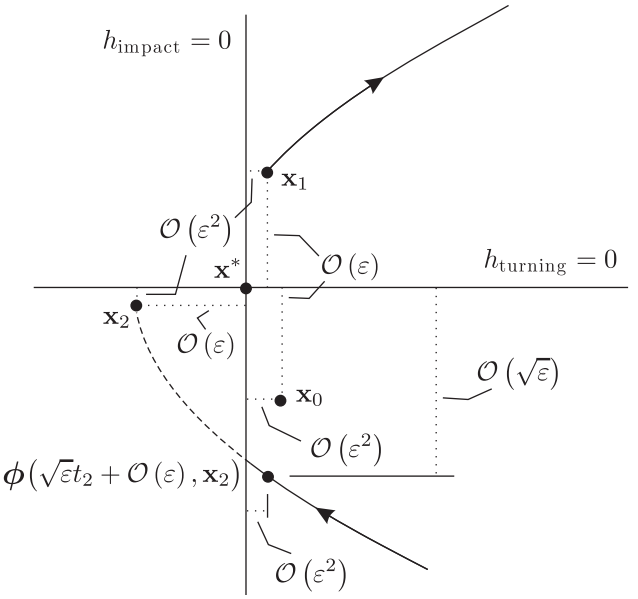

Fig. 3. Schematic illustrating the sequence of points introduced in the derivation of Eq. (24) and the growth in order in ε of the value of h_{turning} at successive impacts.

where $\Omega = \omega_n\sqrt{1-\zeta^2}$. In particular, with

$$t_1 \stackrel{\text{def}}{=} \frac{1}{b\omega^2}\left(\delta\dot{q} - \delta h_{\text{turning}} - \frac{\mathrm{e}^{-2n\pi\zeta\omega_n/\omega}}{\Omega}\begin{pmatrix}(\delta\dot{q} - (1+e)\delta h_{\text{turning}})\Omega\cos\frac{2n\pi\Omega}{\omega}\\ -\omega_n(\omega_n\delta a + \delta\dot{q}\zeta - (1+e)\zeta\delta h_{\text{turning}})\sin\frac{2n\pi\Omega}{\omega}\end{pmatrix}\right) \tag{13}$$

for some positive integer n, it follows that

$$h_{\text{turning}}\left(\boldsymbol{\phi}\left(\frac{2n\pi}{\omega} + \varepsilon t_1 + \mathcal{O}(\varepsilon^2), \mathbf{x}_1\right)\right) = \mathcal{O}(\varepsilon^2) \tag{14}$$

and

$$h_{\text{impact}}\left(\boldsymbol{\phi}\left(\frac{2n\pi}{\omega} + \varepsilon t_1 + \mathcal{O}(\varepsilon^2), \mathbf{x}_1\right)\right) = \delta h_{\text{impact}}\varepsilon + \mathcal{O}(\varepsilon^2), \tag{15}$$

where

$$\delta h_{\text{impact}} = -\delta a + \frac{\mathrm{e}^{-2n\pi\zeta\omega_n/\omega}}{\Omega}\left(\Omega\delta a\cos\tfrac{2n\pi\Omega}{\omega} + (\omega_n\zeta\delta a + \delta\dot{q} - (1+e)\delta h_{\text{turning}})\sin\tfrac{2n\pi\Omega}{\omega}\right). \tag{16}$$

Let n be the smallest integer[1] such that δh_{impact} is negative and set

$$\mathbf{x}_2 = \boldsymbol{\phi}\left(\frac{2n\pi}{\omega} + \varepsilon t_1 + \mathcal{O}\left(\varepsilon^2\right), \mathbf{x}_1\right). \tag{17}$$

It follows that a transversal crossing of h_{impact} must have occurred prior to the trajectory reaching $\mathbf{x}_2$. In particular, with

$$t_2 \stackrel{\text{def}}{=} -\sqrt{-\frac{2\delta h_{\text{impact}}}{b\omega^2}} \tag{18}$$

it follows that

$$h_{\text{impact}}(\boldsymbol{\phi}(\sqrt{\varepsilon}t_2 + \mathcal{O}(\varepsilon), \mathbf{x}_2)) = \mathcal{O}(\varepsilon^2) \tag{19}$$

and

$$h_{\text{turning}}(\boldsymbol{\phi}(\sqrt{\varepsilon}t_2 + \mathcal{O}(\varepsilon), \mathbf{x}_2)) = -\sqrt{-2b\omega^2\delta h_{\text{impact}}}\sqrt{\varepsilon} + \mathcal{O}(\varepsilon), \tag{20}$$

[1] Such an integer is guaranteed to exist in the underdamped case $\zeta < 1$.

whereas

$$\dot{\phi}_2(\sqrt{\varepsilon}t_2 + \mathcal{O}(\varepsilon), \mathbf{x}_2) = \mathcal{O}(\varepsilon) \tag{21}$$

corresponding to the value of absolute velocity, $\dot{q}$, at this location (see Fig. 3).

The above analysis demonstrates that for sufficient small ε, repeated iterations of the three steps described above yield a value of h_{turning} that eventually deviates from 0 by $\mathcal{O}(\sqrt{\varepsilon})$ while $\delta\dot{q}$ remains $\mathcal{O}(\varepsilon)$. It follows that δa and $\delta\dot{q}$ terms in the expression for δh_{impact} may eventually be ignored yielding

$$\delta h_{\text{impact}} = -(1+e)\delta h_{\text{turning}} \frac{e^{-2n\pi\zeta\omega_n/\omega}}{\Omega} \sin\frac{2n\pi\Omega}{\omega} \tag{22}$$

and the map

$$\delta h_{\text{turning}} \mapsto -\sqrt{2b\omega^2(1+e)\delta h_{\text{turning}} \frac{e^{-2n\pi\zeta\omega_n/\omega}}{\Omega} \sin\frac{2n\pi\Omega}{\omega}} \tag{23}$$

from one impact to the next, where n is the smallest integer that guarantees that the argument of the radical is positive.

From Eq. (5), it follows that the jump $\Delta\dot{q}$ in absolute velocity due to impacts is proportional with coefficient $-(1+e)$ to the relative velocity $\delta h_{\text{turning}}$ at impact, thus yielding the map

$$\Delta\dot{q} \mapsto c(e, \omega, b, \omega_n, \zeta)\sqrt{\Delta\dot{q}}, \tag{24}$$

where

$$c(e, \omega, b, \omega_n, \zeta) = \omega(1+e)\sqrt{-2b \frac{e^{-2n\pi\zeta\omega_n/\omega}}{\Omega} \sin\frac{2n\pi\Omega}{\omega}}. \tag{25}$$

3.2. Numerical results

To validate the approximations made in the derivation of the discrete map, Eq. (24), a series of numerical experiments were performed in which data for several successive low-velocity impacts were collected and the value of $\Delta\dot{q}$ at one impact was graphed against the value at the previous impact. Specifically, simulations were performed with the numerical values of ζ, ω_n, and e previously estimated, with $b = 0.65$ mm, and $f = \omega/2\pi = 6$, 10, 14, 18, and 22 Hz. For each set of parameter values, a large number of runs were performed with random initial conditions near $\mathbf{x} = 0$ and with a range of values of a near b. For each run, data were collected for successive impacts as long as $\Delta\dot{q}$ did not exceed 50 mm/s.

Fig. 4 shows a log–log plot of the collected data for the five different excitation frequencies. In each case, a linear regression fit was performed on the data with $\Delta\dot{q} \in (0.01, 1)$ mm/s. The corresponding values of the slope and intercept are shown in tabular form in Table 1. The table further contains predicted values for the slope and intercept (i.e., $\log c(e, \omega, b, \omega_n, \zeta)$) as obtained from Eqs. (24) and (25). The results confirm the validity of the discrete map in predicting the near-grazing transient dynamics.

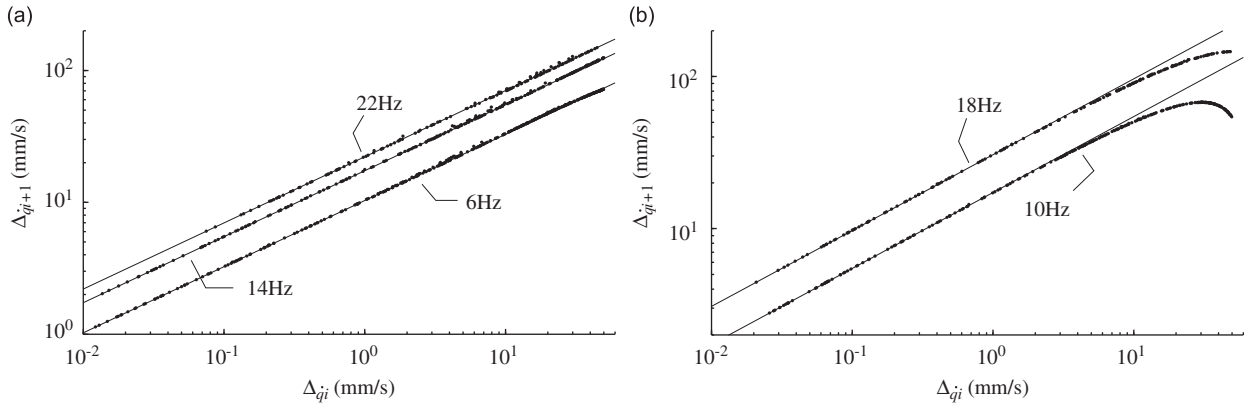

Fig. 4. Numerically simulated $\Delta\dot{q}_{i+1}$ vs. $\Delta\dot{q}_i$ at successive impacts for $\Delta\dot{q} \leqslant 50$ mm/s. Here, straight lines represent linear regression fits performed in the log–log representation using $\Delta\dot{q}_i \in (0.01, 1)$ mm/s corresponding to 77 points for $f = 6$ Hz, 67 points for $f = 10$ Hz, 63 points for $f = 14$ Hz, 57 points for $f = 18$ Hz, and 35 points for $f = 22$ Hz.

Table 1
Comparison of slope and intercept describing the linear fit shown in Fig. 4 and predicted values obtained using Eqs. (24) and (25) with $b = 0.65$.

$\omega/2\pi$ (Hz)	Numerical results		Mapping results	
	Slope	Intercept	Slope	Intercept
6	0.5015	1.0140	0.5	1.0116
10	0.4990	1.2373	0.5	1.2387
14	0.5005	1.2404	0.5	1.2396
18	0.4986	1.4869	0.5	1.4887
22	0.5017	1.3456	0.5	1.3441

Here, $n = 1$ when $\omega = 12\pi$, $n = 2$ when $\omega = 20\pi$ and 28π, and $n = 3$ when $\omega = 36\pi$ and 44π.

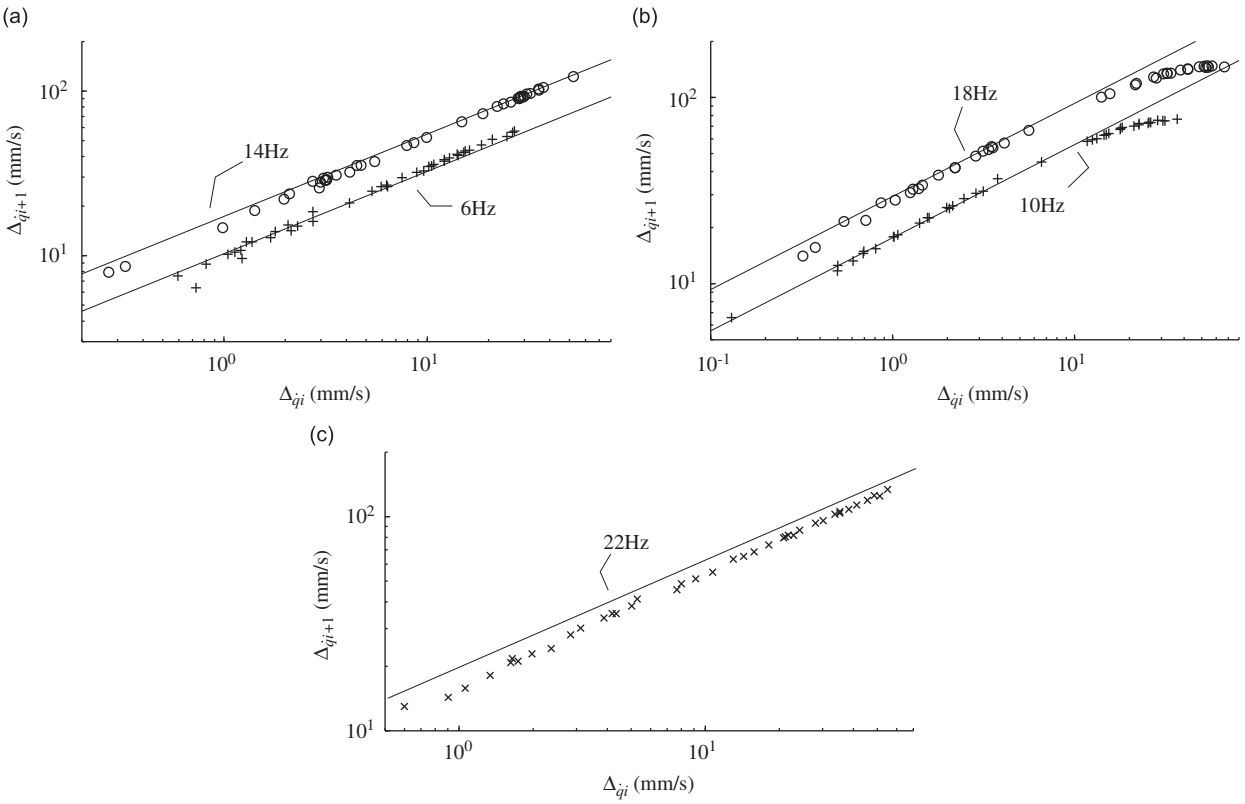

Fig. 5. Experimentally measured values of $\Delta\dot{q}_{i+1}$ vs. $\Delta\dot{q}_i$ collected for three successive impacts. Here, straight lines represent predicted relationship as obtained from Eq. (24).

4. Experimental results

Experiments were performed following the protocol described in Section 2.2 and data were collected and processed in the same manner as described in Section 3.2 with the proviso that for each excitation frequency, the value of b was adjusted to maintain the excitation voltage within an allowable range.

Fig. 5 shows a log–log plot of the collected data for the five different excitation frequencies. In each case, the behavior predicted from Eq. (24) is represented by the included straight lines (where $b = 0.65$ for $f = 6$ and 14 Hz, $b = 0.67$ for $f = 10$ Hz, $b = 0.59$ for $f = 18$ Hz, and $b = 0.54$ for $f = 22$ Hz). The results again confirm the validity of the discrete map in predicting the near-grazing transient dynamics (although a noticeable discrepancy is noticed in the intercept in the case that $f = 22$ Hz). Indeed, the experimental data conform with the predicted value of the integer n, i.e., the smallest integer that guarantees that the argument of the radical in Eq. (25) is positive.

It was observed that the limitations imposed by the measurement hardware and the method for extracting jumps in the absolute velocity made it difficult to collect accurate data for extremely-low-relative-velocity impacts (cf. the leftmost impact in Fig. 6). Indeed, while the discontinuity in the data is still somewhat apparent, the nature of the discontinuity is

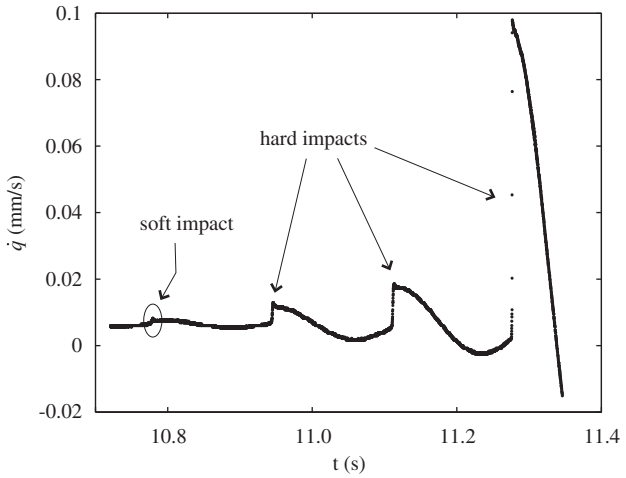

Fig. 6. "Soft" impacts with $\Delta\dot{q}$ below the discernible limit were not included in the processed data.

not as abrupt as in the case of the latter impacts shown in Fig. 6. For this reason, a lower limit was imposed on the values of $\Delta\dot{q}$ included in the analysis.

5. Discussion

The experimental, analytical, and numerical results presented here demonstrate clearly the near-grazing transient behavior that supports the proposed reliance on the nonsmooth fold bifurcation in vibro-impacting systems as the operating principle of a novel class of limit switches. In particular, the increase beyond all bounds of the transient growth rate of near-grazing impact velocities as the threshold parameter value is approached suggests a high sensitivity and rapid switching speed of a corresponding limit switch. In contrast, for limit switches that rely on saddle-node bifurcations of equilibria or smooth cyclic-fold bifurcations of periodic oscillations, the corresponding growth rate would fall off to zero as the threshold value was approached.

Although other investigators have explored the near-grazing dynamics of vibro-impact oscillators, previous work has primarily focused on the form of steady-state attractors and not on the transient behavior following the initial onset of low-relative-velocity impacts [22–27]. As the emphasis here has been on the immediate response of a limit switch following the crossing of the threshold value, only transient results have been included in the analysis. The study of the steady-state behaviors to which the internal state of the switch would be attracted following the initial transient would provide insight into the overall switch design. Work is currently underway to explore this in a coupled vibro-impacting electromechanical circuit.

Recent work on the control of near-grazing dynamics in vibro-impacting systems suggest a mechanism for regulating the limit-switch response [29,30]. With the inclusion of additional feedback, the nonsmooth fold bifurcation associated with near-grazing dynamics can be replaced with the persistence scenario in which a steady-state attractor persists in the vicinity of the threshold parameter value. Such a regulator would enable the inclusion of a secondary fail-safe mechanism that would first need to be triggered in order to enable the limit switch. This would enhance the ability to adjust the sensitivity of the switch to noise and is a suggested topic for further study.

Finally, the present effort also suggests the possibility of relying on the experimental and theoretical formalism as a parameter-identification tool. In particular, while not established with any certainty, we argue that the discrepancy in the intercept shown in Fig. 5(c) is due to misidentified system parameters. Continued work with the present experimental setup as well as with the coupled vibro-impacting electromechanical circuit mentioned above is likely to yield further insight into using the near-grazing transient behavior for system identification.

Acknowledgments

This material is based upon work supported by the National Science Foundation under Grant nos. 0237370 and 0635469 and by the Swedish Science Council under Grant nos. 2003-3699 and 2004-6342.

References

[1] J.-J. Paques, Limit switches: selection for safety, *ISA Transactions* 33 (1) (1994) 99–103.
[2] S. Chatzandroulis, S. Koliopoulou, D. Goustouridis, D. Tsoukalas, Capacitive pressure sensors and switches fabricated using strain compensated SiGeB, *Microelectronic Engineering* 83 (2006) 1209–1211.
[3] I.J. Garshelis, A current threshold sensor, *IEEE Transactions on Magnetics* MAG-15 (6) (1979) 1809–1811.
[4] J. Grohs, M. Mueller, A. Schmidt, A. Uhrig, C. Klingshirn, H. Bartelt, On the possible use of photo thermal optical bistability as a temperature sensor, *Optics Communications* 78 (1) (1990) 77–80.
[5] Y. Li, N. Wu, A low-cost CMOS programmable temperature switch, *Sensors* 8 (5) (2008) 3150–3164.
[6] F.M. Castro, Mechanical switches snap back, *Machine Design* 63 (19) (1991) 56–61.
[7] B. Mi, D.A. Smith, H. Kahn, F.L. Merat, A.H. Heuer, S.M. Phillips, Static and electrically actuated shaped MEMS mirrors, *Journal of Microelectromechanical Systems* 14 (1) (2005) 29–36.
[8] E.M. Abdel-Rahman, A.H. Nayfeh, Secondary resonances of electrically actuated resonant microsensors, *Journal of Micromechanics and Microengineering* 13 (3) (2003) 491–501.
[9] T. Mohr, F.H. Uhlmann, Detecting thresholds by means of jump-phenomena, *7th IEEE International Conference on Electronics, Circuits and Systems, Jounieh, Lebanon*, December 2000, pp. 17–20.
[10] R. Movshovich, B. Yurke, A.D. Smith, A.H. Silver, Subharmonic pumping of a Josephson-parametric amplifier and the pitchfork instability, *Physical Review Letters* 67 (11) (1991) 1411–1414.
[11] I. Siddiqi, R. Vijay, F. Pierre, C.M. Wilson, M. Metcalfe, C. Rigetti, L. Frunzio, M.H. Devoret, RF-driven Josephson bifurcation amplifier for quantum measurement, *Physical Review Letters* 93 (20) (2004) 207002-1–4.
[12] K.L. Turner, R. Baskaran, W. Zhang, Using nonlinear dynamics for performance enhancement in resonant micro and nano-scale devices, *Proceedings of the IEEE Conference on Decision and Control, Maui*, 3, 2003, pp. 2650–2651.
[13] K. Wiesenfeld, B. McNamara, Period-doubling systems as small-signal amplifiers, *Physical Review Letters* 55 (1) (1985) 13–16.
[14] K. Wiesenfeld, B. McNamara, Small-signal amplification in bifurcating dynamical systems, *Physical Review A* 33 (1) (1986) 629–642.
[15] W. Zhang, K.L. Turner, Application of parametric resonance amplification in a single-crystal silicon micro-oscillator based mass sensor, *Sensors and Actuators A* 122 (1) (2005) 23–30.
[16] W. Zhang, R. Baskaran, K.L. Turner, Effect of cubic nonlinearity on auto-parametrically amplified resonant MEMS mass sensor, *Sensors and Actuators A* 102 (1–2) (2002) 139–150.
[17] Y.A. Kuznetsov, *Elements of Applied Bifurcation Theory*, Springer, New York, 2004.
[18] J. Qiu, Z.C. Feng, Parameter dependence of the impact dynamics of thin plates, *Computers and Structures* 75 (5) (2000) 491–506.
[19] X. Zhao, H. Dankowicz, C.K. Reddy, A.H. Nayfeh, Modeling and simulation methodology for impact microactuators, *Journal of Micromechanics and Microengineering* 14 (2004) 775–784.
[20] H. Dankowicz, X. Zhao, Local analysis of co-dimension-one and co-dimension-two grazing bifurcations in impact microactuators, *Physica D* 202 (3–4) (2005) 238–257.
[21] A.B. Nordmark, Non-periodic motion caused by grazing incidence in an impact oscillator, *Journal of Sound and Vibration* 145 (2) (1991) 279–297.
[22] S.R. Bishop, M.G. Thompson, S. Foale, Prediction of period-1 impacts in a driven beam, *Proceedings of the Royal Society A: Mathematical, Physical and Engineering Sciences* 452 (1954) (1996) 2579–2592.
[23] W. Fang, J.A. Wickert, Response of a periodically driven impact oscillator, *Journal of Sound and Vibration* 170 (3) (1994) 397–409.
[24] M.H. Fredriksson, D. Borglund, A.B. Nordmark, Experiments on the onset of impacting motion using a pipe conveying fluid, *Nonlinear Dynamics* 19 (3) (1999) 261–271.
[25] X.H. Long, G. Lin, B. Balachandran, Grazing bifurcations in an elastic structure excited by harmonic impactor motions, *Physica D* 237 (8) (2008) 1129–1138.
[26] P.T. Piiroinen, L.N. Virgin, A.R. Champneys, Chaos and period-adding: experimental and numerical verification of the grazing bifurcation, *Journal of Nonlinear Science* 14 (4) (2004) 383–404.
[27] A. Stensson, A.B. Nordmark, Experimental investigation of some consequences of low velocity impacts in the chaotic dynamics of a mechanical system, *Philosophical Transactions of the Royal Society, Series A* 347 (1683) (1994) 439–448.
[28] J. Eriksson, Experimental and numerical studies of nonsmooth mechanical systems: applications of dimension estimation, Licentiate Thesis, Royal Institute of Technology, Sweden, TRITA-MEK 2005:08, ISSN 0348-467X, 2005.
[29] H. Dankowicz, J. Jerrelind, Control of near-grazing dynamics in impact oscillators, *Proceedings of the Royal Society A: Mathematical, Physical and Engineering Sciences* 461 (2063) (2005) 3365–3380.
[30] H. Dankowicz, F. Svahn, On the stabilizability of near-grazing dynamics in impact oscillators, *International Journal of Robust and Nonlinear Control* 17 (15) (2007) 1405–1429.